PCCP

Accepted Manuscript

ROYAL SOCIETY OF CHEMISTRY

www.rsc.org/pccp

Journal Name

RSCPublishing

ARTICLE

Dual mode quantitative imaging of microscopic viscosity using a conjugated porphyrin dimer†

Cite this: DOI: 10.1039/xoxxoooooox

Aurimas Vyšniauskas,[a] Milan Balaz,[b]‡ Harry L. Anderson[b] and Marina K Kuimova[a]*

Received ooth January 2012,
Accepted ooth January 2012

DOI: 10.1039/xoxxoooooox

www.rsc.org/

Microviscosity is of paramount importance in materials and bio-sciences. Fluorescence imaging using molecular rotors has emerged as a versatile tool to measure microviscosity, either using a fluorescence lifetime or a ratiometric signal of the rotor; however, only a limited number of blue-to-green-emitting fluorophores with both the lifetime and the ratiometric signal sensitivity to viscosity have been reported to date. Here we report a deep red emitting dual viscosity sensor, which allows both the ratiometric and the lifetime imaging of viscosity. We study viscosity in a range of lipid-based systems and conclude that in complex dynamic systems dual detection is preferable in order to independently verify the results of the measurements as well as perform rapid detection of changing viscosity.

Introduction

Viscosity is an important characteristic of a microenvironment, since it determines the micro- and macroscopic properties of materials and controls the rates of processes and reactions on the microscopic scale. The need to detect microscopic viscosity is widely recognised in biochemical and biological research,[1] and new applications are emerging in material and atmospheric sciences.[2–4] Among several methods that allow the detection of viscosity on a microscopic scale, such as fluorescence correlation spectroscopy (FCS),[5,6] fluorescence recovery after photobleaching (FRAP),[7,8] single particle tracking (SPT),[9,10] steady state and time-resolved fluorescence anisotropy,[11–13] detection fluorescence of molecular rotors has secured its place as a versatile technique that allows non-destructive *imaging* of viscosity in heterogeneous samples and on-line detection of *changing* viscosity. These two advantages are not accessible simultaneously with any other existing technique.[14,15] In molecular rotors, the fluorescence competes with intramolecular rotation, which is viscosity dependent. As a consequence, the fluorescence intensity and the fluorescence decay of the excited state are strongly affected by the viscosity of the microenvironment of the probe.

It is now well established that quantitative imaging of viscosity requires either ratiometric detection or fluorescence lifetime measurements, in order to rule out the effect of the concentration of the probe on the observed signal.[16–19] Consequently, both types of molecular rotors, using either ratiometric or lifetime detection, have been reported and used for imaging in a variety of systems, from live cells to lipid membranes to atmospheric aerosols.[2,16–18,20] Here we report a red emitting molecular rotor **1**, Figure 1a, previously synthesized by Balaz et. al.[21] but not explored as a molecular rotor until now. We have discovered that **1** can be used in both modalities of viscosity imaging: lifetime and ratiometric. Only a few dual-mode molecular rotors have been published to date, combining the capabilities of both these approaches.[18,22,23] However, their limited dynamic range for ratiometric measurements complicated the reliable and direct comparison of both techniques in heterogeneous samples. In addition, the blue shifted excitation and emission spectra of these rotors, which contain bands in 400-500 nm range, make them less useful for *in vivo* experiments.

Molecular rotor **1** emits in the red region of the spectrum (640-710 nm, Figure 1), which sets it apart from most existing molecular rotors published to date. In this work we use **1** for measuring viscosity in lipid monolayers, bilayers and in cells. We use these systems to highlight the advantages and limitations of both ratiometric and lifetime approaches. Based on the data for **1** we demonstrate why it might be necessary to have both modalities of quantitative imaging available.

Methods

Calibration of 1

Dimer **1** was synthesised as previously described.[21] A 1 mM solution of the porphyrin dimer in dimethylsulfoxide (DMSO) was used as a stock solution. The viscosity calibration was performed in methanol and glycerol mixtures at room temperature, covering a viscosity range between 0.6 and 1458 cP. Viscosities of the mixtures were measured using Stabinger

viscometer (SVM3000, Anton Paar). All calibration mixtures contained ~0.1% (*v/v*) of DMSO due to using the stock solution of the dye in DMSO. We have confirmed that at such a low concentration DMSO did not affect viscosity measurements. Additionally, DMSO is fully miscible with methanol/glycerol mixtures, which allowed us to rule out the preferential solvation of the dye by DMSO as a potential source of artefacts. Methanol and glycerol were spectroscopic grade obtained from Sigma-Aldrich. Dye solutions for time-resolved fluorescence experiments were prepared by dissolving the required amount of stock solution in a relevant methanol/glycerol mixture and sonicating the solution for two minutes at 40 ˚C to aid full solubilisation of **1**. The final concentration of porphyrin dimer for these measurements was 1.33 µM.

Fluorescence decays were measured using Fluorescence Lifetime Imaging Microscopy (FLIM) setup consisting of a Leica SP 5 II confocal laser scanning microscope; a Coherent Chameleon Vision II mode-locked femtosecond Ti:sapphire laser and a Becker & Hickl SPC-830 (time-correlated single photon counting) TCSPC card. The laser was operating at 80 MHz and producing 140 fs pulses. The output wavelength was tuneable between 680 nm and 1080 nm. The required laser wavelength for one-photon excited fluorescence was obtained by frequency doubling the output of the Ti:sapphire laser with second harmonic generation crystal (SHG, Harmonic, Coherent). 453 nm light was used for exciting the dimer **1**, in order to obtain preferential absorption by the twisted conformer. x20, x40 and x63 objectives were used for measuring the emission of **1** in lipid monolayers, giant unilamellar vesicles (GUVs) and SK-OV-3 cells, respectively. The confocal pinhole was fully opened in order to collect the maximum signal. Fluorescent light was emitted over 600 nm – 750 nm range and detected with a photomultiplier tube (PMC-100-1, Hamamatsu). The light of the desired wavelength was detected by dispersing all emitted light through the prism and changing the width and the position of slits in front of the PMT. 1024 time bins were used for acquiring fluorescence decays. Acquisition times were chosen such that the decays had approximately 10 000 counts at the peak. The instrument response function (IRF) was obtained by recording the scattering curve from a glass coverslip. Dye solutions were kept in Lab-Tek (Nunc, Thermo Scientific) chamber slides during measurements.

Preparation of lipid monolayers

Stock solutions of 1,2-dioleoyl-sn-glycero-3-phosphocholine (DOPC) and 1,2-diphytanoyl-sn-glycero-3-phosphocholine (DPhPC) in chloroform were obtained from Avanti Polar Lipids. A procedure for the preparation of lipid monolayers was adopted from Holden *et al.*[24] Lipid solutions in dodecane were prepared by evaporating chloroform from the required amount of lipid stock solution and then dissolving resulting lipid film in dodecane in order to obtain the final concentration of lipid of 1 mg/mL. Then the stock solution of **1** in DMSO was added, followed by sonication for 5 min at 40 ˚C. The concentration of **1** was 3 µM. 60 µL of 0.11M KCl solution in water was then added into 500 µL lipid and dye mixture in dodecane and the vial was shaken by hand and left to stand for 15 min. Finally, the resulting mixture of water droplets coated in lipid monolayer in dodecane was transferred onto depression slide and imaged.

Preparation of Large Unilamellar Vesicles (LUVs)

Dry lipid-dye film was prepared by evaporating chloroform solution of lipid and **1** mixed at 1000:1 lipid-to-dye ratio. Water was added and the vial was vortexed in order to obtain a uniform suspension. Lipid concentration in the suspension was 1 mg/mL. LUVs were prepared from the suspension by continuously passing the heated suspension at 60 ˚C through Whatman nucleopore track-etched membrane with 200 nm pores using mini-extruder from Avanti Polar Lipids (at least 10 passes).

Preparation of Giant Unilamellar Vesicles (GUVs)

GUVs were prepared by the electroformation method.[25] First, 2 µL of 10 mg/mL lipid and **1** solution in chloroform was spread on ITO (Indium-Tin Oxide) slide on 1 cm^2 area and evaporated under ~2 mPa pressure for 30 min. Lipid-to-dye ratio was 1000. After evaporation, electroformation chamber was assembled from two ITO slides and polydimethylsiloxane (PDMS) spacer, filled with 200 mM sucrose solution in water and connected to the TTi TG550 function generator. Finally, 1.2 V alternating voltage at 10 Hz frequency was applied and the chamber was kept in the oven at 60 ˚C temperature for 1.5 h. The resulting GUVs were transferred into 200 mM glucose solution in water and imaged in a Lab-Tek chamber slide.

Acquisition of fluorescence lifetime images, ratiometric images and fluorescence spectra

FLIM, ratiometric images and fluorescence spectra were all collected using the Leica SPII microscope setup described above. Samples were excited at 453 nm. Fluorescence decays were detected between 620 and 750 nm and 635 - 645 nm decays were used for calibration as described in the Results and Discussion section. FLIM images in lipid monolayers and in GUVs were detected at 650 nm - 660 nm to account for a 15 nm red solvatochromic shift of the fluorescence spectrum of **1** (see Figure S5). FLIM images were acquired at 256x256 pixel resolution using 256 time bins. The scanning frequency was 400 Hz. Ratiometric calibration was performed by dividing two fluorescence images obtained simultaneously using two detectors: 635-645 nm (Detector 1) and 690-700 nm (Detector 2). Ratiometric images of lipid monolayers, GUVs and cells were obtained using 650 – 660 nm and 705-715 nm windows to account for the 15 nm red shift of the spectra. Fluorescence spectra of 10 nm resolution were obtained using the microscope setup by sliding detection window of 10 nm width along wavelength axis by 5 nm and measuring mean fluorescence intensity (λ-scan).

Cell work

SK-OV-3 human ovarian carcinoma cell line was used for cell imaging experiments. Cells were cultured in Dulbecco's modified Eagle's medium (DMEM) with 10% foetal bovine serum (FBS) and split when ~ 70% confluent. 5% CO_2 and 37˚C was used for incubating cells. Cells were seeded into 8-well Lab-Tek chamber for imaging by transferring 50 000 cells per well and allowing them to grow for 24 hours. 10 µM solution of **1** in DMEM with 10% FBS and 1% DMSO was used for staining cells. The cell staining solution was first passed through a 200 nm filter to remove aggregates and warmed in the incubator at 37˚C for 30 min before administering to the cells. The cells were incubated for 24 h and washed 3 times with Hank's Balanced Salt Solution (HBSS) before imaging at 37˚C.

Data analysis

FLIM images were fitted and analysed using FLIMfit software tool developed at Imperial College London (v4.6.1)[26] and Becker & Hickl SPCImage v3.9.7 software. Pixels were binned in order to get around 1000 counts at the peak of each decay. Multiexponential fitting for single decays traces (for the calibration), data processing and analysis was done in MATLAB R2012a and OriginPro 8.6.

Results and Discussion

Butadiyne linked porphyrin dimer **2** was previously shown to have molecular rotor properties, *via* a ratiometric detection method.[17] The working principle of this type of molecular rotor is based on the fact that two fluorescent conformers of a dimer exist, with twisted and planar position of the porphyrin rings, which can interconvert with viscosity dependent rates.[27] Here we tested the molecular rotor properties of **1**, a dimer analogous to **2**, with excellent biocompatibility properties.[28]

The absorption and fluorescence spectra of **1** along with the proposed energy levels diagram are shown in Figure 1b,c. The excitation into higher energy absorption bands (depicted by green dots in either Q or Soret bands) results in the excitation of a twisted conformer,[29] which can either emit light (640 nm, green dot on the insert) or interconvert into a planar form, which emits at 700 nm (red dot on the insert).

The twisted to planar conformer conversion is viscosity-dependent and thus the ratio of the two bands: 640 *vs* 695 nm, can be calibrated against the solution viscosity (Figure 2c), using the Förster-Hoffmann equation.[14,30]

Importantly, the viscosity sensitivity can only be achieved by exciting the dimer preferentially in the twisted conformation (blue arrow in Figure 1c), e.g. at ca 450 nm or 630 nm wavelengths for **1**. Due to the limitations of our experimental setup, in this work we used 453 nm pulsed excitation to prepare the viscosity-sensitive excited state of **1**, however, it is also possible to use the pulsed excitation at 630 nm,[29] which efficiently excites the twisted conformer of **1** and, at the same time, takes full advantage of its red shifted absorption and emission bands that show good overlap with the so-called 'tissue optical window'.

The viscosity-dependent intensity ratio 640:695 nm ranges from 0.05 to 1.6, providing an extremely large dynamic range for ratiometric measurements of viscosity between 1 and 1000 cP. Additionally, both emission bands of the dimer lie in the red region of the spectrum, in the tissue optical window, providing optimal tissue penetration. These two factors set the dimer apart from all other ratiometric rotors available to date and offer significant advantages during live cell and tissue imaging.

Ratiometric viscosity measurements can offer concentration-independent viscosity data as well as extremely fast image recording times; however, they might suffer from artefacts due to environmentally induced shifts in fluorescence or absorption spectra as well as from binding of the probe. On the other hand, the fluorescence lifetime detection method is capable of distinguishing between true viscosity measurements and artefacts, by detecting individual fluorescence decays from all species in the detection volume, thus reporting on undesirable events such as binding or quenching, if present, which reveal themselves as additional exponential component in fluorescence decay. It follows that dual probes, providing advantages of both the ratiometric and the lifetime detection methods, are highly desirable.

Given the interplay of conformer energies shown in Figure 1c we hypothesised that the fluorescence lifetime of the twisted form of **1** is likely to display strong viscosity dependence, due to a twisting originating from this state. We have recorded a series of fluorescence decay traces between 630-730 nm, in methanol/glycerol mixtures of varied viscosity.

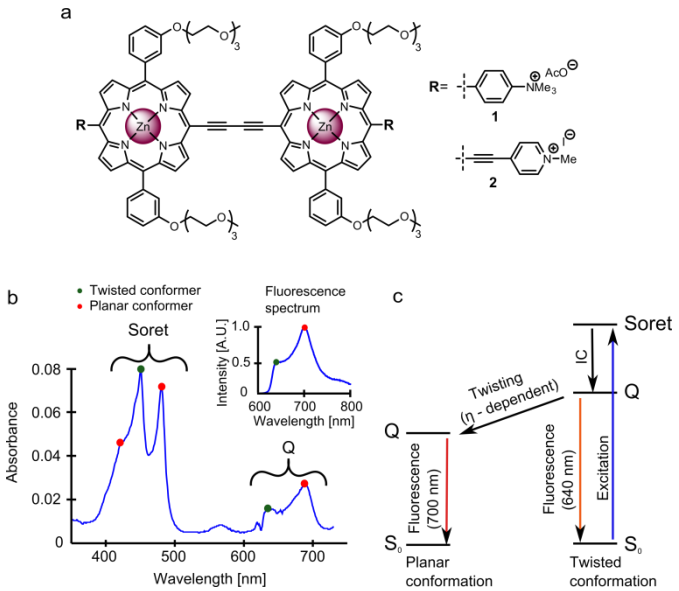

Figure 1. (a) The structure of conjugated porphyrin dimers **1** and **2**. (b) An absorption spectrum of **1** recorded in 6:4 glycerol/methanol mixture and a fluorescence spectrum (insert, λ_{exc} = 453 nm). Green and red dots indicate absorption bands originating from twisted and planar conformers, respectively, in either Q or Soret bands. The viscosity-sensing twisted conformer can be excited in either the Soret (453 nm) or the Q (630 nm) bands. (c) Energy diagram of conformers of **1**. IC – internal conversion.

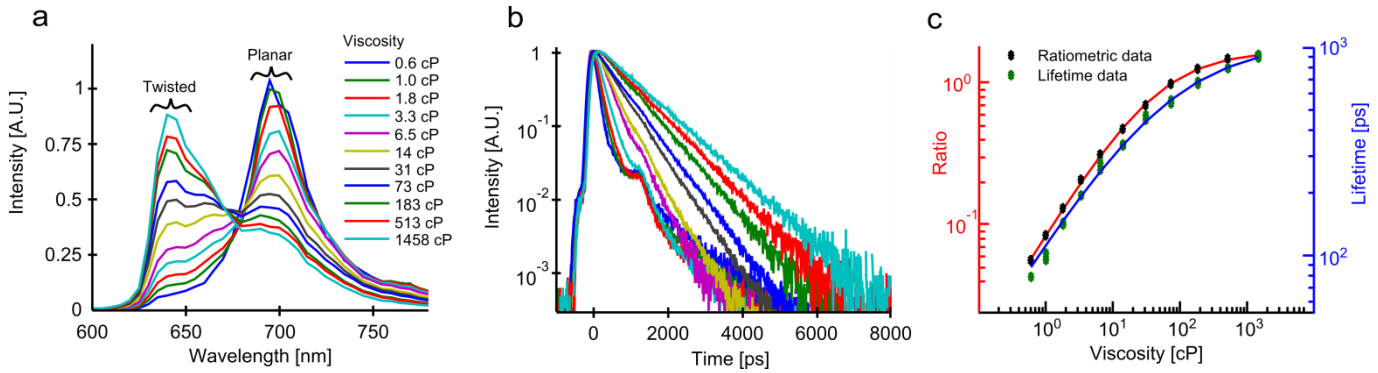

Figure 2. Calibration of **1** in methanol/glycerol mixtures, λ_{exc} = 453 nm. a) Fluorescence spectra. Peaks corresponding to the twisted and the planar conformers are marked. b) Fluorescence decays recorded at 640±5 nm. c) Ratiometric (red) and lifetime (blue) calibration curves.

The representative decays recorded at 640 nm are shown in Figure 2b; the remaining datasets are shown in the Supporting Information (SI), Figure S1. It is clear from this data that at wavelengths below 700 nm the decay traces display a very strong sensitivity to viscosity, with lifetimes between 50 ps and 900 ps, corresponding to a viscosity range 0.6-1500 cP. At the same time, fluorescence decays at and above 700 nm show minimal viscosity dependence, with a decay constant of 900-1000 ps for all viscosities. In the decays above 700 nm the increasing viscosity is manifested by an increase in the decay rise time that varies from 50 to ca 900 ps, matching the decay constants recorded at 640 nm (SI, Figure S2). This match further confirms our proposed photophysical scheme for **1**, giving evidence that the planar conformer does indeed form predominantly from the twisted form. Here it should be noted that, according to the absorption spectra Figure 1b, some proportion of the planar conformer might be directly excited by 450 nm light and its emission spectrum overlaps slightly with the detection window at 640 nm. This results in a biexponential decay (Figure 2b) with a small contribution of the planar decay (< 5% amplitude, SI, Figure S2), consistently observed at 640 nm. The calibration graphs produced for **1**, from both the ratiometric and the lifetime data, Figure. 2c, cover a large dynamic range and conform to the Förster-Hoffmann equation, up to viscosities of ca 800 cP, above which the linearity is lost.

Given that porphyrin dimers such as **1** have an extremely large two photon absorption cross section, up to 2 x 10^5 GM,[28] we performed the ratiometric and lifetime calibration of **1** following two photon excitation, varied between 850 and 950 nm (SI, Figure S3). However, due to poor absorption of two photon light by the twisted conformer[31] because of a loss of conjugation and symmetry, the dynamic range observed in both imaging modalities was significantly reduced compared to the one photon excitation and cannot be considered useful for imaging.

Next, we used **1** for dual mode microviscosity measurements in monolayers at a water/oil interface. Initially **1** was incorporated into a diphytanoylphosphatidylcholine (DPhPC) lipid monolayer surrounding the water droplet in dodecane. DPhPC was chosen as a saturated lipid that exists in liquid-disordered (L_d) phase at room temperature.[32] Fluorescence of **1** was observed only from the dodecane and water interface (SI, Figure S4), confirming the preference of **1** for the lipid phase and/or fluorescence enhancement of **1** in the presence of a more viscous lipid phase. FLIM and ratiometric images were measured, which yielded viscosity maps shown in Figure 3a. Viscosity values were calculated in each pixel using the calibration curves shown in Figure 2c. Unexpectedly, these two methods gave different viscosity values in the monolayer, which were 3.8 cP and 13.3 cP obtained by ratiometric and lifetime imaging, respectively.

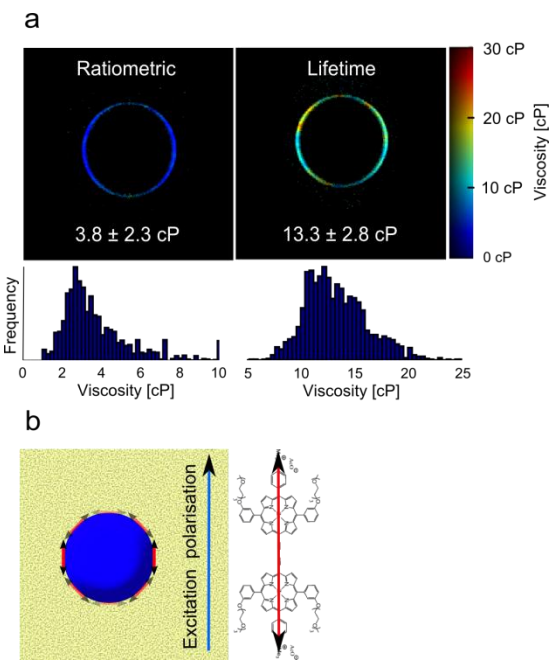

Figure 3. Imaging of **1** in DPhPC lipid monolayers. a) Viscosity maps of DPhPC monolayer at the water/dodecane interface obtained by ratiometric (left) and lifetime (right) methods superimposed on intensity images; λ_{exc} = 453 nm Average viscosity values with the error equal to 1σ and distribution histograms are also shown. b) The schematic showing the relationship between the direction of polarisation of excitation light (blue arrow) and arrangement of the dimer molecules at the interface, resulting in the intensity pattern observed in a). The direction of the transition dipole moment for excitation of the dimer is also shown.

It should be noted that the dominant decay component in FLIM images (responsible for sensing the viscosity) had an amplitude of between 85 – 90% in monolayers, compared to a 95-100 % amplitude recorded in calibration mixtures. The other (longer) decay component was previously assigned to a planar conformer (5% in methanol/glycerol mixtures), and these results indicate that there is a preference for the planar conformation of **1** in lipid monolayer, stronger than prescribed by solution viscosity alone.

To investigate this further we analysed the uneven intensity distribution of the fluorescence of **1** around the water droplet, as shown in Figure 3a: less intense on the top and the bottom and more intense on the sides, while the polarisation of the excitation light was in the image plane as shown by the blue arrow in Figure 3b. These experiments strongly indicate that in Figure 3a the absorption transition dipole moment of **1** is close to being parallel to the polarisation of excitation light at the sides of the droplet (resulting in bright fluorescence) and close to being perpendicular on the top and the bottom of the droplet (resulting in dim fluorescence), Figure 3b. Thus, unexpectedly, **1** preferentially orientates parallel to the water and dodecane interface rather than inserts vertically into the lipid layer. The 15 nm solvatochromic shift of **1** observed in a monolayer compared to methanol/glycerol mixtures (Fig S5, SI), is further confirmation that **1** preferentially localises close to an aqueous environment because the fluorescence spectrum of **1** in water is red-shifted by ~30 nm. Taken together, these results indicate that **1** localises in the lipid head area, close to the aqueous interface, which is likely to favour a planar conformation of a dimer. Since the proportion of the planar form is higher than what can be expected from the viscosity of the environment, the ratiometric method strongly underestimated the viscosity. The lifetime method, however, is not affected and produces a correct viscosity value based on the fluorescence decay fitting. This example clearly shows that care should be taken when quantitatively interpreting ratiometric data.

We have also prepared lipid bilayers as giant unilamellar vesicles (GUVs) and imaged their viscosity by ratiometric and FLIM approaches. In the case of bilayers, **1** demonstrates an increase in viscosity compared to monolayers, by both the ratiometric and the lifetime data (Figure 4). Additionally, **1** reports the same solvatochromic shift as in a monolayer (Figure 4), indicating the same or similar localization of the dye. Thus, even though the dimer is not fully incorporated in the lipid tail region of the bilayer, it senses an increased rigidity of the bilayer structure. Both values obtained with the dimer in the monolayers (13 cP) and in the bilayer (~17 cP), are significantly different to those obtained with the fully imbedded lipid probe, Bodipy, which gave viscosity values of 90 cP (SI, Figure S6) and 160 cP in monolayers and bilayer, respectively.[33] These values are consistent with the lower head region viscosity of a lipid bilayer.[34]

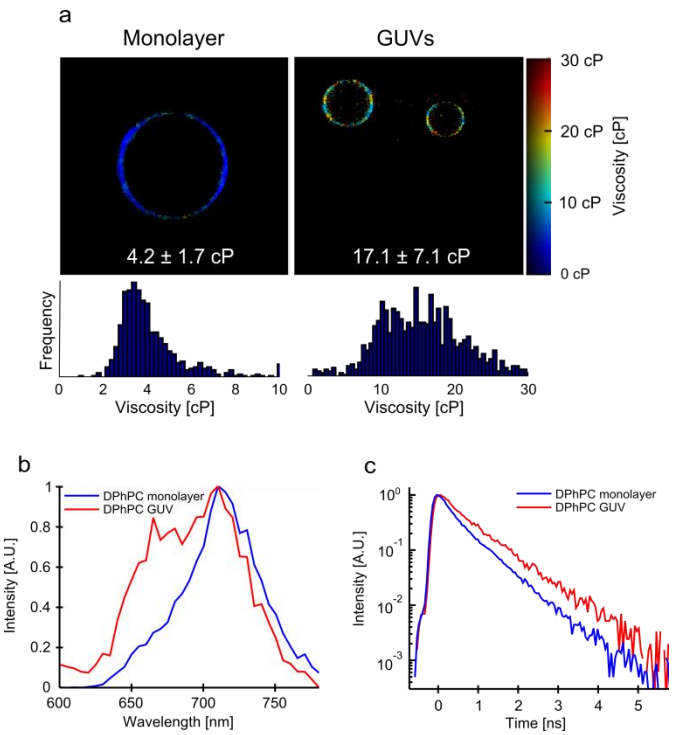

Figure 4. (a) The ratiometric viscosity maps of monolayers and GUVs with corresponding distribution histograms. (b) Fluorescence spectra and (c) fluorescence decays of **1** in DPhPC lipid monolayer (blue) and GUVs (red). In all three cases, **1** measures considerably higher viscosities in GUVs compared to a monolayer, consistent with a more tight packing of lipids in this case. In (c) lifetimes of the twisted conformer correspond to 14 cP and to 17 cP in monolayer and GUVs, respectively.

To utilise the capability for fast image recording available with a ratiometric method, we have tested the effect of singlet oxygen production by the dimer on the viscosity of a monolayer containing an unsaturated lipid, 1,2-dioleoyl-sn-glycero-3-phosphocholine DOPC. Dimer **1** was previously shown to produce singlet oxygen in high yield (ϕ_Δ determined as 0.7 in methanol,[28] although it is expected to be dependent on the excitation wavelength and viscosity and was determined to be as low as 0.2 for the wavelengths directly exciting the twisted conformer in viscous media[29]). Moreover, we have previously demonstrated, using a ratiometric method and a dimer **2** that the viscosity in a single cell increased dramatically during irradiation of the dimer leading to cell death.[17] The results of an irradiation of a DOPC monolayer containing **1** are shown in Figure 5a on the left, and the average viscosity values obtained from these images in Figure 5b. A large viscosity increase of 6 fold is observed, from 4 to 24 cP (ratiometric), which was almost completely supressed in the presence of 0.11M NaN_3, an efficient singlet oxygen quencher (Figure 5a middle). No increase in viscosity was observed in DPhPC without NaN_3 (Figure 5a, right).

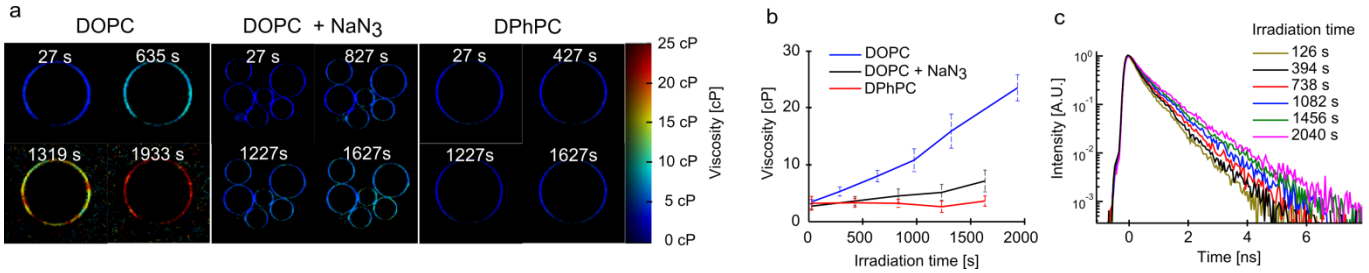

Figure 5. Viscosity increase of DOPC lipid monolayers upon irradiation. a) Viscosity maps of DOPC monolayer (left), DOPC monolayer with 0.11 M NaN_3 added into the aqueous phase (middle) and a DPhPC monolayer (right) at different irradiation times obtained by the ratiometric method. b) Average viscosities as a function of irradiation time obtained from a) Error bars are equal to 1σ. c) Decays from DOPC monolayers at different irradiation times obtained by binning pixels in corresponding FLIM images.

In order to analyse the lifetime data, it was required that all decays were summed to produce a good S/N ratio, Figure 5c. The decays are biexponential and show increasing average lifetime with irradiation time (Figure 5c). Based on the data above we hypothesise that the observed viscosity increase during irradiation of **1** is due to the oxidation of unsaturated lipids with reactive oxygen species (ROS), more specifically singlet molecular oxygen. In spite of the fact that **1** does not fully integrate into the lipid monolayer, an effective oxidation was shown to occur. This interpretation is consistent with no viscosity increase observed in saturated DPhPC lipid or in the presence of NaN_3.

Previously we demonstrated that a porphyrin dimer **2**, structurally similar to **1**, reported a dramatic increase in viscosity during photoinduced cell death, from 50 to 300 cP. Here we set out to test if irradiation of **1** and ensuing PDT produces a similar change in viscosity in cells. **1** was incorporated into SK-OV-3 cells, and the microviscosity was imaged by the ratiometric method, which allows rapid detection of viscosity changes. The results are shown in Figure 6 and demonstrate a 3-fold increase in viscosity in cell cytoplasm upon irradiation, from 5 cP to 13 cP. While the viscosities reported are lower the trend remains the same as for **2**. Due to a low signal and fast bleaching of the dye, viscosity estimation from FLIM images was not possible.

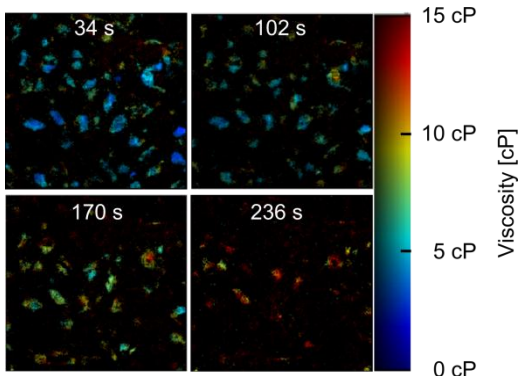

Figure 6. Viscosity maps obtained from ratiometric images of SK-OV-3 cells upon different irradiation times, shown in white above images; λ_{exc} = 453 nm.

Conclusions

In conclusion, we have characterised a red-emitting molecular rotor that works in both the lifetime and the ratiometric measurement modes. We have incorporated the rotor in a range of lipid-based systems and in live cells. We have demonstrated that the combination of both modes allows both quantitative measurements of viscosity and dynamic information to be obtained.

Acknowledgements

AV thanks the EPSRC for the Prize Studentship. MKK is thankful to the EPSRC for the Career Acceleration Fellowship. This work was partially supported by the European Commission in the form of a Marie Curie individual Fellowship to M.B. under the contract MEIT-CT-2006–041522

Notes and references

[a]*Chemistry Department, Imperial College London, Exhibition Road, SW7 2AZ, UK*

[b]*University of Oxford, Department of Chemistry, Chemistry Research Laboratory, Oxford, OX1 3TA, UK*

‡ *Present address: Department of Chemistry, University of Wyoming, Laramie, WY, USA.*

† Electronic Supplementary Information (ESI) available: See DOI: 10.1039/c000000x/

(1) Chauvière, A.; Preziosi, L. Cell Mechanics: From Single Scale-Based Models to Multiscale Modeling (Chapman & Hall/CRC Mathematical & Computational Biology); Chapman and Hall/CRC, 2010.

(2) Hosny, N. A.; Fitzgerald, C.; Tong, C.; Kalberer, M.; Kuimova, M. K.; Pope, F. D. Faraday Discuss. **2013**, 165, 343–356.

(3) Nölle, J. M.; Jüngst, C.; Zumbusch, A.; Wöll, D. Polym. Chem. **2014**, 5, 2700–2703.

(4) Hungerford, G.; Allison, A.; McLoskey, D.; Kuimova, M. K.; Yahioglu, G.; Suhling, K. J. Phys. Chem. B **2009**, 113, 12067–12074.

(5) Schwille, P. Cell Biochem. Biophys. **2001**, 34, 383–408.

(6) Magde, D.; Elson, E.; Webb, W. W. Phys. Rev. Lett. **1972**, 29, 705–708.

(7) Swaminathan, R.; Hoang, C. P.; Verkman, A. S. Biophys. J. **1997**, 72, 1900–1907.

(8) Poo, M.-M.; Cone, R. A. Nature **1974**, 247, 438–441.

(9) Kaji, N.; Ogawa, R.; Oki, A.; Horiike, Y.; Tokeshi, M.; Baba, Y. Anal. Bioanal. Chem. **2006**, 386, 759–764.

(10) Levi, V.; Gratton, E. Cell Biochem. Biophys. **2007**, 48, 1–15.
(11) Dix, J. A; Verkman, A. S. Biophys. J. **1990**, 57, 231–240.
(12) Siegel, J.; Suhling, K.; Lévêque-Fort, S.; Webb, S. E. D.; Davis, D. M.; Phillips, D.; Sabharwal, Y.; French, P. M. W. Rev. Sci. Instrum. **2003**, 74, 182–192.
(13) Fushimi, K.; Verkman, A. S. J. Cell Biol. **1991**, 112, 719–725.
(14) Kuimova, M. K. Phys. Chem. Chem. Phys. **2012**, 14, 12671–12686.
(15) Haidekker, M. A.; Nipper, M.; Mustafic, A.; Lichlyter, D.; Dakanali, M.; Theodorakis, E. A. Dyes with Segmental Mobility: Molecular Rotors; Demchenko, A. P., Ed.; Springer Series on Fluorescence; Springer Berlin Heidelberg: Berlin, Heidelberg, 2010; Vol. 8, pp. 267–308.
(16) Kuimova, M. K.; Yahioglu, G.; Levitt, J. A.; Suhling, K. J. Am. Chem. Soc. **2008**, 130, 6672–6673.
(17) Kuimova, M. K.; Botchway, S. W.; Parker, A. W.; Balaz, M.; Collins, H. A.; Anderson, H. L.; Suhling, K.; Ogilby, P. R. Nat. Chem. **2009**, 1, 69–73.
(18) Peng, X. J.; Yang, Z. G.; Wang, J. Y.; Fan, J. L.; He, Y. X.; Song, F. L.; Wang, B. S.; Sun, S. G.; Qu, J. L.; Qi, J.; Yang, M. J. Am. Chem. Soc. **2011**, 133, 6626–6635.
(19) Haidekker, M. A; Brady, T. P.; Lichlyter, D.; Theodorakis, E. A. J. Am. Chem. Soc. **2006**, 128, 398–399.
(20) Haidekker, M. A; Ling, T.; Anglo, M.; Stevens, H. Y.; Frangos, J. A; Theodorakis, E. A. Chem. Biol. **2001**, 8, 123–131.
(21) Balaz, M.; Collins, H. A.; Dahlstedt, E.; Anderson, H. L. Org. Biomol. Chem. **2009**, 7, 874–888.
(22) Yang, Z.; He, Y.; Lee, J.-H.; Park, N.; Suh, M.; Chae, W.-S.; Cao, J.; Peng, X.; Jung, H.; Kang, C.; Kim, J. S. J. Am. Chem. Soc. **2013**, 135, 9181–9185.
(23) Jiang, N.; Fan, J.; Zhang, S.; Wu, T.; Wang, J.; Gao, P.; Qu, J.; Zhou, F.; Peng, X. Sensors Actuators B Chem. **2014**, 190, 685–693.
(24) Holden, M. A; Needham, D.; Bayley, H. J. Am. Chem. Soc. **2007**, 129, 8650–8655.
(25) Angelova, M. I.; Dimitrov, D. S. **1986**, 303–311.
(26) Warren, S. C.; Margineanu, A.; Alibhai, D.; Kelly, D. J.; Talbot, C.; Alexandrov, Y.; Munro, I.; Katan, M.; Dunsby, C.; French, P. M. W. PLoS One **2013**, 8, e70687.
(27) Winters, M. U.; Karnbratt, J.; Eng, M.; Wilson, C. J.; Anderson, H. L.; Albinsson, B. J. Phys. Chem. C **2007**, 111, 7192–7199.
(28) Kuimova, M. K.; Collins, H. A.; Balaz, M.; Dahlstedt, E.; Levitt, J. A.; Sergent, N.; Suhling, K.; Drobizhev, M.; Makarov, N. S.; Rebane, A.; Anderson, H. L.; Phillips, D. Org. Biomol. Chem. **2009**, 7, 889–896.
(29) Kuimova, M. K.; Balaz, M.; Anderson, H. L.; Ogilby, P. R. J. Am. Chem. Soc. **2009**, 131, 7948–7949.
(30) Forster, T.; Hoffmann, G. Zeitschrift Fur Phys. Chemie-Frankfurt **1971**, 75, 63–76.
(31) Wilkinson, J. D.; Wicks, G.; Nowak-Król, A.; Łukasiewicz, Ł. G.; Wilson, C. J.; Drobizhev, M.; Rebane, A.; Gryko, D. T.; Anderson, H. L. J. Mater. Chem. C **2014**, 2, 6802.
(32) Lindsey, H.; Petersen, N. O.; Chan, S. I. Biochim. Biophys. Acta **1979**, 555, 147–167.
(33) Wu, Y.; Stefl, M.; Olzyńska, A.; Hof, M.; Yahioglu, G.; Yip, P.; Casey, D. R.; Ces, O.; Humpolíčková, J.; Kuimova, M. K. Phys. Chem. Chem. Phys. **2013**, 15, 14986–14993.
(34) Yeagle, P. L. The Structure of Biological Membranes, Second Edition; CRC Press, 2004.